

11A.6 EXPLORING HODOGRAPH-BASED TECHNIQUES TO ESTIMATE THE VELOCITY OF RIGHT-MOVING SUPERCELLS

Hamish A. Ramsay* and Charles A. Doswell III ⁽¹⁾
CIMMS / School of Meteorology, University of Oklahoma, Norman, Oklahoma
⁽¹⁾ CIMMS, University of Oklahoma, Norman, Oklahoma

1. INTRODUCTION

Since a simple supercell motion forecasting scheme was developed in the mid-1970's (Maddox 1976), several other algorithms have been put forth of varying complexity (Colquhoun 1980; Davies and Johns 1993; Davies 1998; Rasmussen and Blanchard 1998; Bunkers et al. 2000). To be able to forecast supercell motion accurately is important, since supercells are often accompanied by severe and potentially fatal weather such as tornadoes, flash flooding, large hail and damaging wind gusts. Of additional importance is the application of supercell motion estimates to related severe weather parameters, including storm-relative helicity (SRH) (Davies-Jones 1984; Davies-Jones et al. 1990) and storm-relative winds (Brooks et al. 1994), both of which aid in assessing the likelihood of supercell development, as well as tornado intensity.

Each supercell motion algorithm depends on some combination of wind profile-related variables. These variables, in turn, depend upon arbitrary parameters: essentially the top and bottom levels of the mean wind layer, the top and bottom levels of the vertical wind shear layer, and an empirically-derived deviation vector (often used as a constant). The arbitrary nature of these parameters should be a concern to the forecaster, who may use these algorithms with little or no awareness of the sensitivities associated with them. The atmosphere is dynamic, and homogeneity is the exception rather than a rule, so it makes sense that any particular algorithm may perform differently, given a change in the local environmental conditions.

The sensitivity of storm motion estimates to these arbitrary parameters is the primary issue to be explored in the current study. A secondary objective is to test whether information from a sounding, namely the Lifting Condensation Level (LCL), the Level of Free Convection (LFC), and the Equilibrium Level (EL), can be used to define the top and bottom level of the mean wind and/or shear layer, and thereby possibly reduce the arbitrary nature of those parameters.

2. SUPERCELL MOTION FORECAST SCHEMES

Maddox (1976, hereafter M76) analyzed 159 tornado proximity soundings, defined to be within 92.5

km of a verified tornado which occurred between 1600 and 1900 (CST). Having considered previous studies concerning deviate severe storm motions (Marwitz 1972; Fankhauser 1971), Maddox estimated the average motion of a right-moving supercell to be at 30° to the right of the mean sounding direction and at 75% of the mean sounding speed (denoted hereafter as 30R75). The mean sounding wind was computed by taking the average of the non-pressure-weighted observed winds at the surface (SFC), 850, 700, 500, 300, and 200 hPa levels.

Colquhoun (1980, hereafter C80) estimated the velocity of severe storms by equating the mass of air brought into the storm by both the updraft and the downdraft. Some restrictive assumptions are that, (1) the air brought into storm by the updraft is balanced by the air brought out of the storm by the downdraft, (2) that the upper limit of the downdraft is 450 hPa; (3) maximum storm intensity is reached when it moves with the motion giving the maximum rate of inflow into the storm; (4) in a storm-relative framework, the updraft approaches from the front and the downdraft from the back, or vice versa. The method was originally tested using a sample of ten severe thunderstorm proximity soundings, which resulted in an average absolute direction error of 4.5 degrees and a mean vector error (MVE) of 1.9 m s^{-1} .

Davies and Johns (1993, hereafter DJ93) modified Maddox's method using a sample of 31 right-moving supercell proximity soundings. They did this by stratifying the storm motion according to the mean environmental wind speed in the SFC (0 km)-6-km layer. For relatively strong mean wind environments (i.e., 0-6-km mean wind > 30 knots), it was found that the storms moved on average at 20 degrees to the right of the mean wind, and at 85% of the speed of the mean wind. Similarly, for environments characterized by weaker mean winds (i.e., 0-6-km mean wind \leq 30 knots), the storms moved closer to 30R75, as originally proposed by Maddox.

Davies (1998, hereafter D98) extended his earlier work by including supercells in environments where the 0-6-km mean wind was less than 20 knots. A sample of 23 twelve-hour forecast proximity soundings was examined, and it was found that the observed storm motion was generally far to the right of 0-6-km mean wind, and greater than 30 degrees in directional deviation. Thus, the 30R75 method was deemed to be inappropriate for such weak wind environments. As an alternative, a 'sliding scale' algorithm was suggested in which the 0-6-km mean wind was partitioned into three divisions; (1) speed \geq 30 knots, (2) speed 20-29 knots and (3) speed 10-19 knots. Evidence was shown to

* Corresponding author address: Hamish A. Ramsay, CIMMS/School of Meteorology, University of Oklahoma, 100 East Boyd, Norman, OK 73019-1013; e-mail: hramsay@rossby.metr.ou.edu

support supercells, and even violent tornadoes, in 0-6-km mean wind fields as weak as 10-12 knots.

Rasmussen and Blanchard (1998, hereafter RB98) developed an algorithm based on 45 supercell proximity soundings. The representative hodographs were translated so that the 0-500-m mean wind (assumed to be the boundary layer, BL) was at the origin, and the BL-4-km shear vector was aligned with the + u axis. Forecast storm motion was estimated at 8.6 m s^{-1} orthogonal and to the right of the tip of the $0.6\mathbf{S}$ vector, where \mathbf{S} is the BL-4-km shear vector. Unlike other methods discussed thus far, this method is Galilean invariant. This principle has been applied in several numerical modeling studies (Rotunno and Klemp, 1982, 1985; Weisman and Klemp, 1982, 1984), which show that supercell motion depends on properties of the vertical wind shear, and not just the mean wind, defined through an arbitrary layer. Therefore, the RB98 scheme predicts the same shear-relative forecast motion, regardless of where the hodograph lies with respect to the origin.

Most recently, Bunkers et al. (2000) have developed the so-called 'Internal Dynamics' (ID) method for predicting supercell motion. Like RB98, the technique is Galilean invariant, and is based partly on the modeling work done by Rotunno and Klemp (1982, 1985). Rotunno and Klemp demonstrated that enhanced vertical motion, owing to shear-induced vertical pressure gradients, is biased toward the right of the vertical wind shear vector for clockwise-turning hodographs. Consequently, the algorithm has been established on the assumption that supercell motion can be divided into an advection component and a propagation component. Using a dataset of 130 right-moving supercells, Bunkers found that the ID method yielded the lowest MVE when the following parameters were used: (1) a 0-6-km (0-8-km) non-pressure-weighted (pressure-weighted) mean wind; (2) an orthogonal deviation from the 0-6-km mean wind of 7.5 m s^{-1} ; (3) a 5.5-6-km average wind for the head of the vertical wind shear vector, and (4) a 0-500-m average wind for the tail of the vertical wind shear vector. Use of the Bunkers method has rapidly become widespread, and on April 21 2000, NCEP incorporated this algorithm into its ETA model storm relative helicity calculations.

3. DATA AND METHODOLOGY

The basic dataset consists of 524 supercell proximity soundings and radar-observed storm motions, extending from 1958 to 2002, and covering a large area of the continental United States. These were partitioned into two sets of data: (1) a reference dataset comprising 130 cases (as used by Bunkers et al. (2000) to develop the 'ID method') and (2) a new dataset comprising 394 cases. It should be also noted that the observed storm motions and associated proximity soundings, used to compile the new dataset, were part of a larger dataset provided by M. Bunkers. However, unlike the reference dataset, only observations from a single sounding location were selected.

The criteria used to define 'proximity' were similar to that used by Bunkers et al. (2000) and Thompson (1998). To be included in the new dataset, each sounding had to be:

- i) within 100 nautical miles of the supercell
- ii) released within ± 3 hours from the time of the supercell
- iii) in the inflow region of the supercell
- iv) uncontaminated by nearby convection
- v) uncontaminated by the passage of fronts and other boundaries

3.1 Sensitivity Testing

The M76 method's sensitivity to its parameters was evaluated by varying the angular deviation and fractional portion of mean wind speed, as well as the depth of the mean wind layer. For example, the fractional portion of the mean wind speed was varied from 50 % to 100 %, and the depth of the mean wind layer was varied from 0-6 km to 0-12 km. The mean wind velocity for each layer was calculated using both pressure-weighting and non-pressure-weighting techniques.

The C80 algorithm was tested by varying the upper limit of the mass-flux integral used to compute the mean wind. Storm motions were computed using the original upper limit of 450 hPa, as well as 500, 400, 350, 300, 250 and 200 hPa.

Following the work of M76, DJ93 partitioned the observed storm motions into two groups, according to whether the environmental 0-6-km non-pressure-weighted mean wind was (i) greater than 15 m s^{-1} , or (ii) less than 15 m s^{-1} . The proposition that supercells should deviate less than 30° to the right of the 0-6-km mean wind when the mean wind speed averages more than 15 m s^{-1} was tested using the new data set.

The RB98 algorithm was tested using a number of different values for the parameters: \mathbf{S} , the fractional length of \mathbf{S} , and the orthogonal deviation vector (D). The depth of the vertical wind shear layer was varied from BL-3 km, to BL-8 km in one kilometer increments. The fractional length of the vertical wind shear vector, calculated for each layer, was also varied from 0.2 to 1.0. Finally, the magnitude of the deviation vector was varied using values ranging from 6 m s^{-1} to 10 m s^{-1} (orthogonal and to the right of the shear vector).

According to Bunkers et al. (2000), the equation for the velocity of a right-moving supercell can be expressed as:

$$(1) \quad \mathbf{V}_{\text{RM}} = \mathbf{V}_{\text{mean}} + D \left[\frac{\frac{\partial \mathbf{V}}{\partial z} \times \mathbf{k}}{\left| \frac{\partial \mathbf{V}}{\partial z} \right|} \right]$$

where \mathbf{V}_{mean} is the mean wind vector, $\frac{\partial \mathbf{V}}{\partial z}$ is the vertical wind shear vector, and D is the magnitude of the deviation vector from the tip of the mean wind vector, and which is confined to be perpendicular and to the right of the vertical shear vector.

The sensitivity of the algorithm was explored by considering different values for the top and bottom levels of the mean wind layer, the top and bottom levels of the vertical wind shear layer, and D . For instance, the bottom of the mean wind layer was varied from the SFC to 2 km in 500 m increments, while the top was varied from 3 km to 12 km in 1 km increments. In addition to these somewhat arbitrary levels, the mean wind layer was also defined by using the LCL, LFC and EL. The vertical wind shear layer and D were varied in a similar fashion.

3.2 The Offset Scheme

The forecast errors of the five forecast schemes revealed varying amounts of bias and dispersion, depending partly on the layer chosen to compute the mean wind. Since the mean winds and the observed storm motions are known, it was possible to work backwards to explore the relationship between the two. A preliminary analysis of the forecast errors in the other schemes has shown that a significant part of the total error was associated with the bias in the forecasts. That bias can be computed easily by subtracting the observed $u-v$ median from the forecasted $u-v$ median. An 'offset' vector then was defined as the vector difference between the medians of the mean wind and the observed motion scatters. This vector was used as a constant to offset each point in the mean wind scatter to produce a motion estimate, having zero bias.

3.3 Kernel Density Estimation

Kernel Density Estimation (hereafter, KDE) is a non-parametric technique whereby a known density function (the kernel) is applied to each data point in the distribution, and then summed to produce a smooth, continuous estimate of the true density of the empirical distribution. The 'kernel' is the function used in the smoothing procedure, and can take on a variety of forms including a triangle, a rectangle, or a Gaussian curve. In the current study, a Gaussian kernel was used to create an estimate of the two-dimensional scatters. The KDE technique was found to be a powerful tool, as it produced a simple graphical summary of the empirical distribution, and allowed for easy examination of the dispersion and bias associated with each set of forecast errors. Most importantly, the KDE allowed for several distributions to be displayed and interpreted easily on the same plot.

4. RESULTS

4.1 The Bunkers Scheme

The storm motion forecast errors in the Bunkers scheme were most sensitive to changes in the non-pressure-weighted mean wind layer. A non-pressure-weighted mean wind layer of less than 0-8 km resulted in an underestimate of the u -component of motion, whereas a layer deeper than 0-8 km resulted in an overestimate (Fig. 1). The forecast v -component of

motion proved to be more or less independent of the depth of the mean wind layer; its bias ranged from + 0.6 to + 1.2 m s^{-1} . The non-pressure-weighted mean wind layer that yielded the lowest median vector error (2.9 m s^{-1}), as well as the least bias, was 0-8 km.

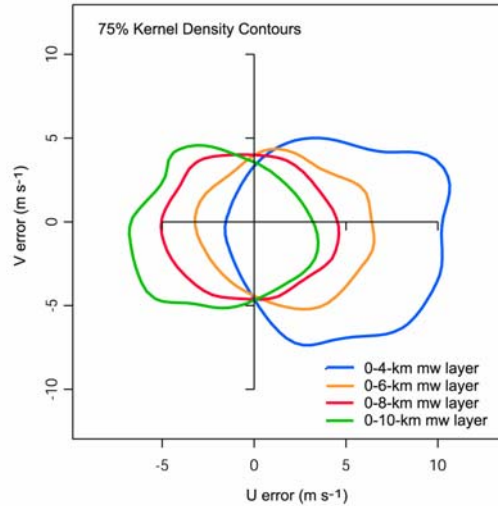


Figure 1. KDE plot showing vector error distributions for the 0-4, 0-6, 0-8, and 0-10-km non-pressure-weighted mean wind layers in the Bunkers scheme.

When pressure-weighting was employed to calculate the mean wind, the variance in the $u-v$ component bias in the errors decreased significantly, particularly between 0-6-km and 0-10-km. The median vector error ranged between 2.9 m s^{-1} and 8.7 m s^{-1} using a 0-12-km mean wind layer and a 0-3-km layer respectively. Both the minimum median and mean vector errors were found using the 0-12-km mean wind layer. This result is in substantial disagreement with Bunkers et al. (2000), in which it was posited that the minimum MVE was found using either a 0-7 or a 0-8-km pressure-weighted mean wind layer.

It was found that the inclusion of information other than the hodograph to define the top and bottom levels of the mean wind layer, such as the LCL and the EL, offered no further reduction in the forecast errors than when using arbitrary fixed heights. It was the pressure-weighted SFC-EL mean wind layer that resulted in the lowest median vector error (3.1 m s^{-1}), which was only slightly larger than the minimum median errors associated with both the 0-8-km non-pressure-weighted and 0-12-km pressure-weighted layers (2.9 m s^{-1}). The propinquity of the errors between the SFC-EL and 0-12-km layers was probably the consequence of the average EL being located at close to 12 km. Furthermore, the SFC-EL pressure-weighted layer resulted in substantially less dispersion and bias than both the LCL-EL and LFC-EL mean wind layers (Fig. 2). Evidently, the Bunkers scheme results in better forecasts for a mean wind layer that originates

somewhere below the lifting condensation level, and preferably at the surface.

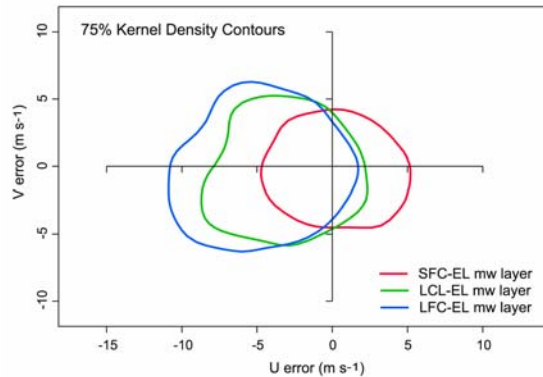


Figure 2. KDE plot showing distribution of vector errors using the SFC-EL, LCL-EL, and LFC-EL layers to define the pressure-weighted mean wind layer in the Bunkers scheme.

The layer through which the vertical wind shear was calculated was found to have the least effect on the bias and dispersion of the forecast errors (Fig. 3). Indeed, the median vector error remained almost constant for a wide range of vertical wind shear layers. It was interesting to note that the forecast errors were more sensitive to changes in the bottom of the vertical wind shear layer given a constant top, rather than vice versa (not shown). The lowest median vector error was found using vertical wind shear layers ranging from BL-(5.5-6 km) to BL-(7.5-8 km).

The magnitude of the deviation vector (D) was found to play a major role in determining the v -component of the forecast motion (Fig. 4). Apparently, this is due to the constraint in Eq. (1) that the deviation vector must be orthogonal and to the right of the vertical wind shear vector, which is often oriented from left to right across the hodograph. Apart from the apparent bias in the v -component of motion, Fig. 4 shows little variation in the size of the kernel density estimates. Accordingly, the storm motion errors were reduced by using D values ranging between 7 and 9 m s^{-1} . The lowest bias in both the u and the v component of motion was found using a D of 8 m s^{-1} . The minimum median vector error was found by using a D of 7.5-8.0 m s^{-1} , as established in the original Bunkers scheme.

4.2 The RB98 Scheme

The depth of the vertical wind shear layer in the RB98 scheme had a direct effect on both the median vector error and the bias in the u -component of the estimated motion. It was found that, for a given deviation vector, the BL-5-km and BL-6-km shear layers resulted in the lowest median vector errors of 3.7 m s^{-1} (Table 1). In addition, the application of shear layers outside the range of BL-4 km to BL-6 km led to decreased accuracy in the forecasts, even when the u - v bias was removed. These results extend the work of

RB98, in which a BL-4-km bulk shear vector was used with no apparent justification.

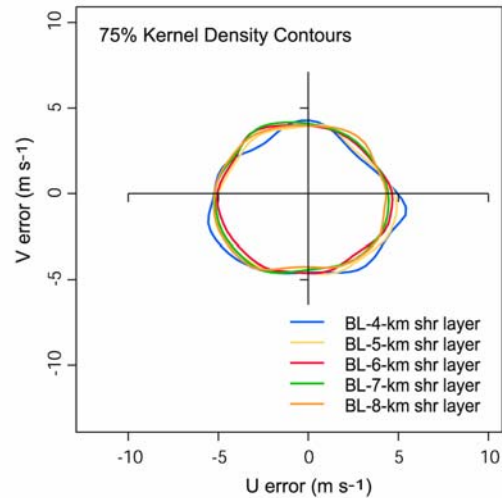


Figure 3. KDE plot showing vector error distributions using various vertical wind shear layers in the Bunkers scheme.

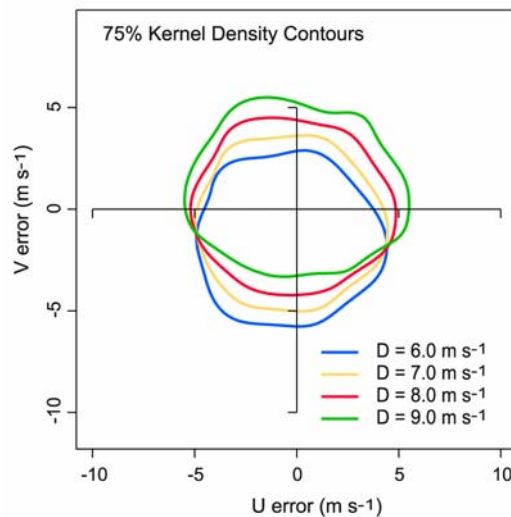


Figure 4. KDE plot showing distribution of forecast errors using different D values from the 0-8-km non-pressure-weighted mean wind.

The magnitude of the deviation vector determined essentially the v -component of the forecast motion. Like the Bunkers scheme, the deviation vector was confined to be perpendicular and to the right of the vertical wind shear vector, which most often oriented itself from left to right across the hodograph. It was found that a deviation vector of between 7 m s^{-1} and 7.5 m s^{-1} resulted in the minimum v -component bias, and the minimum median vector error, when coupled with the BL-5-km bulk shear layer (Table 1). The optimum

deviation vector differed from that used in RB98, which asserted that the best empirical fit to the storm motions was obtained using a deviation vector of 8.6 m s^{-1} .

Bulk Shear Layer	Deviation from Bulk Shear Layer				
	6 m s^{-1}	7 m s^{-1}	7.5 m s^{-1}	8.6 m s^{-1}	10 m s^{-1}
BL-3 km	5.9	5.7	5.6	5.6	6.0
BL-4 km	4.4	4.2	4.3	4.4	5.1
BL-5 km	3.7	3.7	3.7	3.9	4.6
BL-6 km	3.7	3.7	3.9	4.0	4.7
BL-7 km	4.6	4.4	4.4	4.9	5.6
BL-8 km	5.5	5.7	5.7	5.8	6.5

Table 1. Median vector errors for various combinations of D and bulk shear layer in the RB98 scheme.

4.3 The M76 Scheme

The M76 scheme was sensitive to the depth of the non-pressure-weighted mean wind layer. For example, a motion of 30R75 (30 degrees to the right of the mean wind, and 75% of its speed) resulted in the minimum MVE when a 0-10-km non-pressure-weighted mean wind was employed. However, when the mean wind was calculated using a shallower layer, the 30R75 method resulted in an underestimate of both the rightward deviation in direction from the mean wind, and the speed of motion. For instance, it was found that when using a 0-6-km non-pressure-weighted mean wind, the forecast errors were minimized by using directional deviations ranging from 30° to 40° to the right of the mean wind, and speed deviations between 85% and 100%. Furthermore, it was found that the median u -component of the mean wind had a tendency to increase as the depth of the mean wind layer increased, while the v -component remained almost constant. Thus, there was a tendency for the angle between the observed storm motion and the mean wind to increase as the mean wind layer decreased.

Evidently, the minimum MVE associated with the 0-10-km mean wind layer (4.5 m s^{-1}) was 1 m s^{-1} less than the corresponding error associated with the 0-6-km mean wind layer (5.5 m s^{-1}). This result suggests that, despite the apparent differences in the mean deviant direction and speed, the method is more suitably applied to relatively deep non-pressure-weighted mean wind layers.

4.4 The DJ93 Scheme

Following DJ93, the observed storm motions were stratified according to the magnitude of the 0-6-km non-pressure-weighted mean wind speed. The current work supports the idea that the amount to which the storm motions deviate from the 0-6-km mean wind depends upon the magnitude of the mean wind speed, at least by angle. For weaker mean wind fields (i.e., 0-6-km mean wind $< 15 \text{ m s}^{-1}$) it was found that the storms deviated on average 40R105, whereas for stronger mean wind fields (i.e., 0-6-km mean wind $> 15 \text{ m s}^{-1}$), the mean deviant motion was closer to DJ93's original suggestion of 25R85 (see Fig. 5 for a qualitative illustration of this difference).

These results are inconsistent with the original DJ93 scheme. We find a tendency for the 0-6-km mean wind field to underestimate the speed of the storm motion when the magnitude of the wind field is less than 15 m s^{-1} . Furthermore, the fractional proportion of the mean wind used to forecast the storm motion was shown to *increase* as the mean wind field decreased. DJ93 found the opposite result.

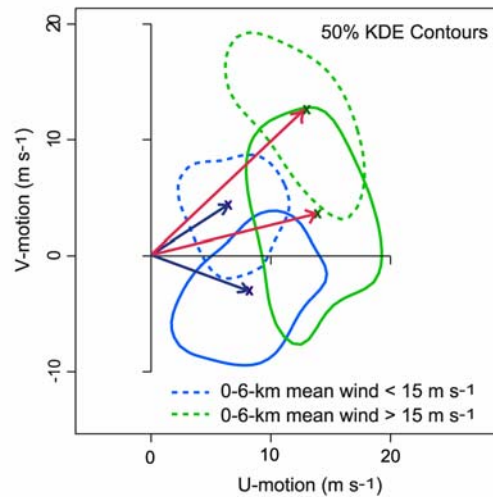


Figure 5. Observed storm motions (solid KDE contours) stratified by the magnitude of the 0-6-km non-pressure-weighted mean wind speed. Dashed KDE contours show observed 0-6-km mean wind for speeds less than (blue) and greater than (green) 15 m s^{-1} .

4.5 The C80 Scheme

Despite being the most computationally sophisticated of all the forecast algorithms, the C80 scheme produced considerably large errors (Table 2). The u -component of the estimated storm motion was regulated largely by the depth of the integrated wind field. On the other hand, the v -component was found to be relatively insensitive to this parameter. The minimum forecast error was found by using the integrated SFC-350-hPa mass flux layer. This result extends the

original C80 scheme, in which only the SFC-450-hPa layer was used. In addition, the forecast errors obtained for the new dataset were about 5 m s^{-1} larger than those presented in the original paper. C80 found an average absolute directional error of 4.5° and a mean vector error of 1.9 m s^{-1} .

	M76	C80	RB98	Bunk.	Off.
MVE	4.5	7.2	4.0	3.4	4.6
MDVE	4.1	6.2	3.7	2.9	4.2
Min VE	0.2	0.3	0.2	0.2	0.1
Max VE	14	25.7	16.0	12.3	15.6
St. Dev.	2.6	4.5	2.5	2.3	2.9

Table 2. Summary statistics of the vector errors (m s^{-1}) for each scheme, using the parameters that yielded the ‘optimum’ forecast. Median vector error is denoted MDVE

4.6 The Offset Scheme

The MVE associated with the offset vector for each non-pressure-weighted mean wind layer was shown to be relatively insensitive to changes in the mean wind layer, as it was varied from 0-6 km to 0-12 km (Fig. 6). Indeed, the minimum MVE was obtained using the 0-8-km layer, with an associated offset vector of $(-0.7 \mathbf{i} - 7.1 \mathbf{j}) \text{ m s}^{-1}$. This result is consistent with the optimum deviation vector magnitude obtained in both the Bunkers and RB98 schemes. The latter schemes impose an additional shear-relative directional constraint on the offset vector, which is the fundamental difference between them and this simple scheme. Further, the v -component of the offset vector for each layer remained relatively constant, at around 7 m s^{-1} , while the u -component varied from $+1.8$ to -3.9 m s^{-1} (Fig. 6). The minimum in error dispersion associated with the 0-8-km layer suggests that this may be the most representative layer, on the average, to estimate the advection component of supercell motion, but the differences among the layers are minor.

4.7 Comparing the Forecast Schemes.

In terms of general forecast performance, the revised Bunkers scheme resulted in the minimum forecast error (MDVE = 2.9 m s^{-1}), and was more accurate than the other schemes for 135 out of 394 cases (Table 3). The revised RB98 scheme resulted in the second lowest forecast error (MDVE = 3.7 m s^{-1}), while both the Offset and M76 schemes performed comparatively well (MDVE = 4.1 m s^{-1}). The relatively strong correlation ($r = 0.68$) of the forecast errors in Bunkers and RB98 schemes confirms their qualitative similarity. The C80 scheme performed demonstrably worse than the other schemes, as evidenced by the large forecast errors associated with it (MDVE = 6.2 m s^{-1}).

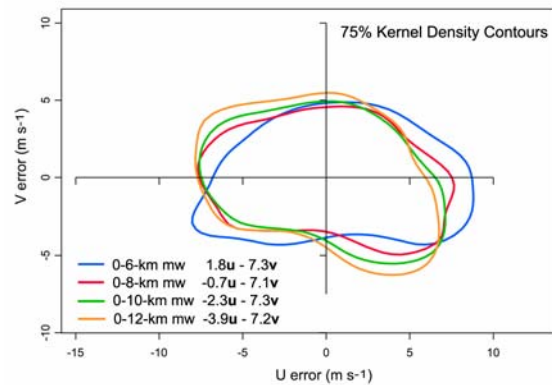


Figure 6. KDE plot showing the errors associated with empirically derived offset vectors from various non-pressure-weighted mean wind layers.

Although the Bunkers and RB98 schemes resulted in the best storm motion estimates, on average (Fig. 7), for any given day it was difficult to know which scheme to use (Table 3). Additional information obtained from the sounding did not help to reduce this uncertainty. Indeed, all the forecast schemes were capable of producing both very small forecast errors (less than 0.3 m s^{-1}) and very large forecast errors (greater than 12 m s^{-1}), as shown in Table 2. The difficulty lies in determining the environments conducive to these extremes.

Scheme	1st	2nd	3rd	4th	5th
Bunkers	135	120	81	44	9
RB98	99	84	72	77	57
Offset	65	72	93	88	67
M76	67	71	92	113	39
C80	23	39	44	63	214

Table 3. Frequency of the relative accuracy of the forecast schemes when compared head to head. 1st designates the minimum vector error per event and 5th designates the maximum vector error.

The Bunkers scheme was shown to be statistically superior to its nearest competitor, RB98, as well as the other schemes, based on the Wilcoxon Signed-Rank test ($\mu \neq 0$, $Z = -6.196$, $p < 0.00001$). The test is designed to determine not only how many times a particular scheme ‘wins’, but how much it wins by when it does.

The superiority of the Bunkers and RB98 schemes was greatest for hodographs in which the wind profile deviated significantly from the mean. For a subset of 41 ‘atypical’ hodographs, defined arbitrarily as those with either a 0-6-km mean wind speed of less than 5 m s^{-1} , or

a 0-10-km v -component of less than -10 m s^{-1} , the Bunkers and RB98 schemes resulted in MVEs of 3.1 and 3.4 m s^{-1} respectively, whereas the other schemes performed considerably worse (Table 4)

4.8 Some General Observations Regarding the New Dataset.

The observed storm motions varied in direction from north-northeasterly to southwesterly; however most were clustered in the first and second quadrants of the hodograph. Interestingly, a small subset of supercells moved toward the southwest. It was found that such atypical storm motions were generally accompanied by deep northerly or northwesterly flow. However, the average proximity hodograph was characterized by a southeasterly wind at the surface, a south-southwesterly wind at 850 hPa , and a general west-southwesterly flow aloft. The wind profile just described closely resembles the proximity hodographs shown in Maddox (1976), and the idealized quarter-circle hodograph often used in numerical supercell simulations (Weisman and Rotunno 2000).

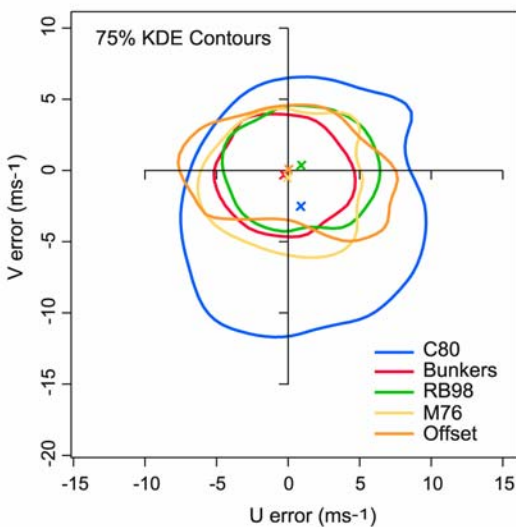


Figure 7. KDE plot showing the distribution of forecast errors for each optimum scheme. Medians denoted by 'X'.

Although most of the supercells deviated to the right of the mean wind, regardless of which mean wind layer was used, there were six cases in which the supercells deviated to the right of the 0-6-km mean wind vector, but to the left of the 0-8, 0-10 and 0-12-km mean winds. This is an interesting result, since it raises questions about the definition of a 'right-moving' supercell, discussed further in the next section.

The angle between the observed storm motion and the 0-6-km mean wind vector was found to increase as the magnitude of the 0-6-km mean wind decreased. The average *magnitude* of the deviation vector (absolute vector difference between the observed

motion and the mean wind) was about 9 m s^{-1} , and was independent of the 0-6-km mean wind speed (Fig. 8). Hence, there was little predictive relationship between the length of the deviation vector and the mean wind speed alone.

A similar absence of a prognostic relationship was shown to exist between the 0-6-km shear magnitude (the length of the shear vector) and the observed storm motion deviation from the 0-6-km mean wind vector (Fig. 9). The 0-6-km shear magnitude ranged from 15 m s^{-1} to 95 m s^{-1} , with a mean around 42 m s^{-1} . There was a slight tendency for the observed deviation magnitude to increase as the shear magnitude increased ($r = 0.26$).

5. Discussion

It has been shown that the majority of the right-moving supercells presented herein are associated with strong clockwise turning of the wind vector between the surface and 700 hPa . Indeed, it is theorized (Rotunno and Klemp 1982) that this clockwise turning of the wind field with height promotes the development of a cyclonic right-moving storm. This theory is the underlying premise behind the deviation term in Bunkers scheme, as seen in Eq. (1).

Despite the relative accuracy of the Bunkers scheme, there were times in which it produced large errors ($> 10 \text{ m s}^{-1}$). These errors suggest that supercell storm motion is determined by more than just the mean wind and the vertical wind shear. In fact, it was found that most of the large errors in the Bunkers scheme were associated with either high-precipitation (hereafter, HP) supercells, or supercells that eventually evolved into bow echoes. Likewise, RB98 suggested that, based on climatological data, HP supercells have a tendency to deviate significantly more than their predicted motion, and that such deviation did not appear to be related to the vertical wind shear in the lowest half of the troposphere. Other studies have shown that HP supercells have a proclivity to develop and move along pre-existing thermal boundaries, including old outflow boundaries and stationary fronts (Moller et al. 1990). This may in part explain some of the large forecast errors in the Bunkers scheme.

Given such external influences, it was somewhat surprising that the forecast errors were found to be as low as they were. There are many factors, peripheral to the mean wind and the vertical wind shear parameters, which have been shown to influence supercell motion (Maddox et al. 1980; Zehr and Purdom 1982; Moller et al 1990, Guyer 2002; Sills et al. 2004). Furthermore, it has been shown that the optimum values of the parameters in the Bunkers scheme, and others, do not always yield an accurate forecast. Consequently, selecting the most suitable mean wind and/or vertical wind shear layer to be used in these schemes is a nontrivial issue. Bunkers et al. (2000) suggested that a mean wind layer less than 0-6 km may be more suitable for shallow or low-topped supercells.

TYPICAL HODOGRAPHS (N=353)					
	C80	M76	RB98	Bunkers	Offset
MVE (m s ⁻¹)	7.2	4.4	4.1	3.5	4.5
MDVE (m s ⁻¹)	5.9	3.9	3.8	2.9	4.0
ATYPICAL HODOGRAPHS (N=41)					
	C80	M76	RB98	Bunkers	Offset
MVE (m s ⁻¹)	6.8	4.9	3.4	3.1	5.3
MDVE (m s ⁻¹)	6.6	5.2	3.1	2.9	4.8

Table 4. Mean vector error and median vector error for each optimum scheme using 353 typical hodographs and 41 atypical hodographs.

However, indications from the current study do not support this hypothesis. By similar logic, a mean wind layer deeper than 0-6 km may be more appropriate for environments characterized by extreme buoyancy or a deep troposphere. Again, little evidence has been found to support this notion here. In fact, it was found that for a given equilibrium level, and a given scheme, the mean wind layer yielding the minimum forecast error ranged anywhere from 0-3 km to 0-10 km. This issue was explored further by allowing the depth of the mean wind layer to be determined by information other than the hodograph (i.e., the LCL, LFC and the EL) rather than arbitrary fixed heights. The possible advantages of making the mean wind a function of one or more the above parameters has been ruminated in previous studies (Bunkers et al. 2000; Davies and Johns 1998), though never tested. For the first time then, the current work has shown that the use of information other than the hodograph results in no better estimate of the storm motion than using the hodograph alone. In fact, it was found that that forecast errors increased substantially when using the LCL-EL or LFC-EL to calculate the mean wind, rather than the SFC-EL.

This result was somewhat surprising, since it has been suggested that the advective component of motion ought to be confined to the cloud-bearing layer (Weaver, 1979; Zehr and Purdom, 1982), so that the winds between the cloud base and the ground should have little effect.

It is of interest to examine how each of the storm motion estimation schemes compare when the when the wind profile resides away from the top right quadrant of the hodograph. It has been shown that the Galilean invariant, shear-relative schemes, such as Bunkers and RB98, can be superior to the other schemes for 'atypical' hodographs, or for cases in which the average tropospheric flow is north-northwesterly. Hence, the Bunkers and RB98 schemes produce the same shear-relative storm motion estimate, regardless of where the hodograph lies with respect to the origin.

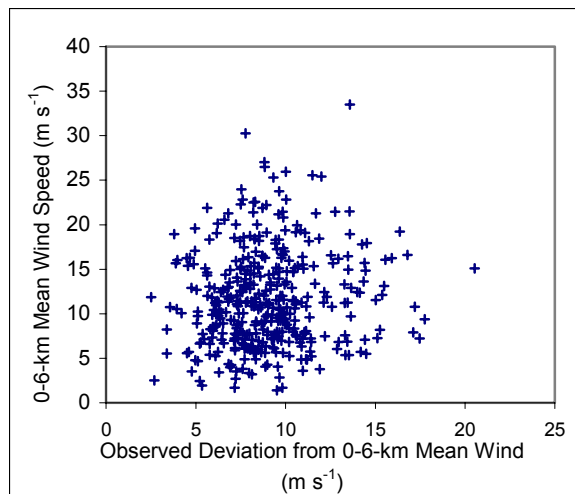


Figure 8. Scatter plot of observed magnitude of supercell deviation from 0-6-km mean wind vs. 0-6-km mean wind speed.

As Bunkers pointed out, the relative accuracy of the M76 scheme in the past has been mostly attributable to the fact that the average supercell proximity wind profile has an inclination to reside in the top-right quadrant of the hodograph. Indeed, the current study indicates that for such hodographs, the error difference between the Bunkers and M76 schemes is less.

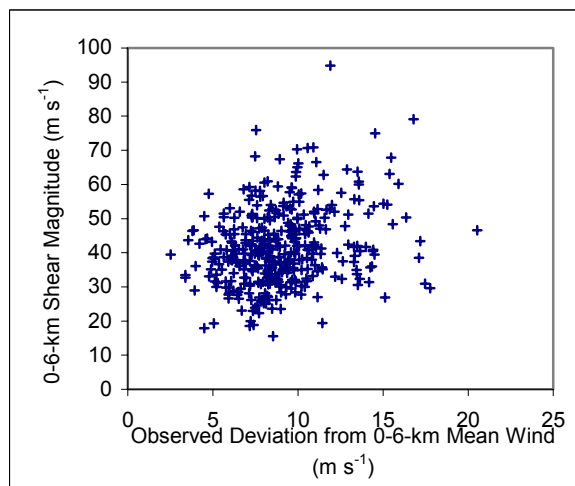


Figure 9. Scatter plot of observed magnitude of supercell deviation from 0-6-km mean wind vs. 0-6-km shear magnitude

However, when the wind profile (and hence the vertical shear vector) is confined to the lower quadrants of the hodograph, or when the mean wind is relatively weak, the Bunkers and RB98 schemes perform substantially better than the schemes based on the mean wind alone.

Despite the apparent advantages of using a shear-relative forecast scheme with a fixed deviation vector, the observed storm motions revealed only a weak linear relationship between deviation from the 0-6-km mean wind and the magnitude of the 0-6-km vertical wind shear. This suggests that the vertical wind shear is only one of several factors contributing to the propagation component of supercell motion. Indeed, Weaver (1976) suggested that supercell motion may be influenced by pre-existing boundary layer convergence zones, as well as outflow boundaries produced by the storms themselves. Other authors (Maddox et al. 1980; Zehr and Purdom 1982; Moller et al. 1990; Marshall et al. 2002) have demonstrated that supercells have a tendency to move along well defined low-level thermal gradients such as warm fronts and sea-breezes.

6. SUMMARY AND CONCLUSIONS

Five supercell motion estimation schemes were explored with respect to their arbitrary hodograph-analysis parameters, and compared with one another. The Offset scheme, though not a forecast scheme, was developed to examine a simple relationship between the mean wind and the observed storm motion by removing the bias in the mean-wind-estimated forecast.

The Bunkers scheme proved to be slightly superior to the other schemes in terms of the minimum MDE/MDVE. However, it was necessary to modify the mean wind parameters specified in the original Bunkers scheme in order to find the minimum MDVE (2.9 m s^{-1}). The use of the LCL, LFC and EL to define the mean wind layer led to larger forecast errors than when using arbitrary fixed heights, such as 0-8 km. In fact, it was found that the inclusion of the winds in the sub-cloud layer was necessary to obtain the minimum forecast errors for the Bunkers scheme. On the basis of the results presented herein, it is suggested that the original Bunkers scheme be revised by changing the non-pressure-weighted mean wind layer from 0-6 km to 0-8 km.

The RB98 scheme resulted in the second lowest forecast errors, and was found to give results similar to the Bunkers scheme. The apparent success of these forecast schemes may be due to their Galilean-invariant, shear-relative properties. This is particularly evident for supercells within wind profiles that deviate significantly from the composite supercell hodograph. Nevertheless, there were times in which both the Bunkers and RB98 schemes yielded considerably large forecast errors. It was found that these larger errors were often associated with high-precipitation supercells, or supercells with characteristic bow echo structures.

The M76 and Offset schemes demonstrated comparable estimation accuracy, despite their qualitative differences. It has been shown that when applying the M76-type schemes, it is advantageous to use a deep non-pressure-weighted mean wind layer (i.e., 0-10 km or deeper). Furthermore, the M76 scheme revealed a propensity for the angle between the mean wind vector and the observed storm motion to increase as the magnitude of the mean wind decreased.

The offset scheme was found to work best using the same mean wind layer and deviation magnitude as used in the Bunkers scheme. That the Bunkers scheme yielded a more accurate motion estimate than the Offset scheme, on average, was most likely due to the difference in deviant direction, since all other parameters were equal.

Finally, the C80 scheme performed demonstrably worse than the other forecast schemes when compared head to head, and this is highlighted by its relatively large MDVE. It is not recommended that this scheme be used in operational forecasting.

The current work has effectively demonstrated that forecasting the motion of supercell storms is a complex issue. This complexity is due to the fact that supercell environments vary considerably. Thus, even the most successful schemes should be approached with caution. There are many, many factors that contribute to supercell motion. Furthermore, the schemes are based on the assumption that the proximity hodograph is an appropriate representation of the actual environment in which the storm forms. Indeed, trying to define what constitutes the most suitable 'proximity' sounding has been shown to be a problematic issue (Brooks et al. 1994). It is suggested that the influence of features not observed by the hodograph, such as outflow boundaries, warm fronts and sea-breezes, may account for some degree of the forecast errors associated the forecast schemes investigated herein. Still, this is beyond the scope of the current work, and remains to be explored in future research.

Acknowledgements: Authors gratefully acknowledge the project funding provided by NOAA/CIMMS, and valuable contributions from Matthew Bunkers (NWS), John Hart (SPC), Harold Brooks (NSSL), Mike Richman (OU), Lance Leslie (OU), and Evgeni Fedorovich (OU).

7. REFERENCES

- Achtemeier, G.L., 1969: Some observations of splitting thunderstorms over Iowa on August 25–26, 1965. Preprints, *Sixth Conf. on Severe Local Storms*, Chicago, IL, Amer. Meteor. Soc., 89–94.
- Atkins, N.T., M.L. Weisman, and L.J. Wicker, 1999: The influence of pre-existing boundaries on supercell evolution. *Mon. Wea. Rev.*, **127**, 2910-2927.
- Brooks, H.E., C.A. Doswell III and J. Cooper, 1994: On the environments of tornadic and nontornadic mesocyclones. *Wea. Forecasting*, **9**, 606–618.
- Brooks, H.E., and C.A. Doswell III, 1996: A comparison of measures-oriented and distributions-oriented approaches to forecast verification. *Wea. Forecasting*, **11**, 288–303.
- Brooks, H.E., C.A. Doswell III, and M.P. Kay, 2003: Climatological estimates of local daily tornado

- probability for the United States. *Wea. Forecasting*, **18**, 626–640.
- Brown, Rodger A. 1993: A compositing approach for preserving significant features in atmospheric profiles. *Mon. Wea. Rev.*, **121**, 874–874.
- Browning, K.A., 1964: Airflow and precipitation trajectories within severe local storms which travel to the right of the winds. *J. Atmos. Sci.*, **21**, 634–639.
- Browning, K.A., 1965: The evolution of tornadic storms. *J. Atmos. Sci.*, **22**, 664–668.
- Browning, K.A., and R.J. Donaldson Jr., 1963: Airflow and structure of a tornadic storm. *J. Atmos. Sci.*, **20**, 533–545.
- Browning, K.A., 1965: Some inferences about the updraft within a severe local storm. *J. Atmos. Sci.*, **22**, 669–677
- Bunkers, M.J., B.A. Klimowski, J.W. Zeidler, R.L. Thompson, and M.L. Weisman, 2000: Predicting supercell motion using a new hodograph technique. *Wea. Forecasting*, **15**, 61–79.
- Charba, J., and Y. Sasaki, 1971: Structure and movement of the severe thunderstorms of 3 April 1964 as revealed from radar and surface mesonet network data analysis. *J. Meteor. Soc. Japan*, **49**, 191–214.
- Colquhoun, J.R., 1980: A method of estimating the velocity of a severe thunderstorm using the vertical wind profile in the storm's environment. Preprints, *Eighth Conf. on Weather Forecasting and Analysis*, Denver, CO, Amer. Meteor. Soc., 316–323.
- Darkow, G.L., 1969: An analysis of over sixty tornado proximity soundings. Preprints, *Sixth Conf. on Severe Local Storms*, Chicago, IL, Amer. Meteor. Soc., 218–221.
- Davies, J.M., 1998: On supercell motion in weaker wind environments. Preprints, *19th Conf. on Severe Local Storms*, Minneapolis, MN, Amer. Meteor. Soc., 685–688.
- Davies, J.M., and R.H. Johns, 1993: Some wind and instability parameters associated with strong and violent tornadoes. Part I: Wind shear and helicity. *The Tornado: Its Structure, Dynamics, Prediction, and Hazards, Geophys. Monogr.*, No. 79, Amer. Geophys. Union, 573–582.
- Davies, J.M., 2002: Significant tornadoes in environments with relatively weak shear. Preprints, *21st Conf. on Severe Local Storms*, San Antonio, TX, Amer. Meteor. Soc., 651–654
- Davies-Jones, R., 2002: Linear and nonlinear propagation of supercell storms. *J. Atmos. Sci.*, **59**, 3178–3205.
- Droegemeier, K.K., S.M. Lazarus, and R. Davies-Jones, 1993: The influence of helicity on numerically simulated convective storms. *Mon. Wea. Rev.*, **121**, 2005–2029.
- Evans, J.S., and C.A. Doswell III, 2001: Examination of Derecho Environments Using Proximity Soundings. *Wea. Forecasting*, **16**, 329–342.
- Guyer, J.L., 2002: A case of supercell intensification along a preexisting boundary – Clay county Nebraska tornado of 22 September 2001. Preprints, *21st Conf. on Severe Local Storms*, San Antonio, TX, Amer. Meteor. Soc., 579–581.
- Johns, R.H., 1984: A synoptic climatology of northwest-flow severe weather outbreaks. Part II: Meteorological parameters and synoptic patterns. *Mon. Wea. Rev.*, **112**, 449–464.
- Johns, R.H., J.M. Davies, and P.W. Leftwich, 1993: Some wind and instability parameters associated with strong and violent tornadoes. Part II: Variations in the combinations of wind and instability parameters. *The Tornado: Its Structure, Dynamics, Prediction, and Hazards, Geophys. Monogr.*, No. 79, Amer. Geophys. Union, 583–590.
- Klemp, J.B., and R.B. Wilhelmson, 1978: Simulations of right- and left-moving storms produced through storm splitting. *J. Atmos. Sci.*, **35**, 1097–1110.
- Klemp, J.B., 1987: Dynamics of tornadic thunderstorms. *Ann. Rev. Fluid Mech.*, **19**, 369–402.
- Maddox, R.A., 1976: An evaluation of tornado proximity wind and stability data. *Mon. Wea. Rev.*, **104**, 133–142.
- Maddox, R.A., L.R. Hoxit, and C.F. Chappell, 1980: A study of tornadic thunderstorm interactions with thermal boundaries. *Mon. Wea. Rev.*, **108**, 322–336.
- Markowski, P.M., J.M. Straka, E.N. Rasmussen, and D.O. Blanchard, 1998: Variability of storm-relative helicity during VORTEX. *Mon. Wea. Rev.*, **126**, 2959–2971.
- Marshall, T.P., C. Broyles, S. Kersch and J. Wingenroth, 2002: The effects of low-level boundaries on the development of the Panhandle, TX tornadic storm on 29 May 2001. Preprints, *21st Conf. on Severe Local Storms*, San Antonio, TX, Amer. Meteor. Soc., 559–562.
- Marwitz, J.D., 1972a: The structure and motion of severe hailstorms. Part I: Supercell storms. *J. Appl. Meteor.*, **11**, 166–179.
- Moller, A.R., C.A. Doswell III, and R. Przybylinski, 1990: High-precipitation supercells: A conceptual model and

- documentation. Preprints, *16th Conf. on Severe Local Storms*, Kananaskis Park, AB, Canada, Amer. Meteor. Soc., 52–57.
- Monteverdi, J. P., W. Blier, G. Stumpf, W. Pi, and K. Anderson, 2001: First WSR-88D documentation of an anticyclonic supercell with anticyclonic tornadoes: The Sunnyvale–Los Altos, California, tornadoes of 4 May 1998. *Mon. Wea. Rev.*, **129**, 2805–2814.
- Moller, A.R., C.A. Doswell III, M.P. Foster, and G.R. Woodall, 1994: The operational recognition of supercell thunderstorm environments and storm structures. *Wea. Forecasting*, **9**, 327–347.
- Murphy, A.H., and D.S. Wilks, 1998: A case study of the use of statistical models in forecast verification: precipitation probability forecasts. *Wea. Forecasting*, **13**, 795–810.
- Newton, C.W., and J.C. Fankhauser, 1964: On the movements of convective storms, with emphasis on size discrimination in relation to water-budget requirements. *J. Appl. Meteor.*, **3**, 651–668.
- Rasmussen, E.N., and D.O. Blanchard, 1998: A baseline climatology of sounding-derived supercell and tornado forecast parameters. *Wea. Forecasting*, **13**, 1148–1164.
- Rotunno, R., and J.B. Klemp, 1982: The influence of the shear-induced pressure gradient on thunderstorm motion. *Mon. Wea. Rev.*, **110**, 136–151.
- Rotunno, R., and J.B. Klemp, 1985: On the rotation and propagation of simulated supercell thunderstorms. *J. Atmos. Sci.*, **42**, 271–292.
- Sills, D. M., J. Wilson, P.I. Joe, D.W. Burgess, R.M. Webb, and N.I. Fox, 2004: The 3 November tornadic event during Sydney 2000: Storm evolution and the role of low-level boundaries. *Wea. Forecasting*, **19**, 22–42.
- Stumpf, J., A. Witt, D.E. Mitchell, P.L. Spencer, J.T. Johnson, M.D. Eilts, K.W. Thomas, and D.W. Burgess, 1998: The National Severe Storms Laboratory Mesocyclone Detection Algorithm for the WSR-88D*. *Wea. Forecasting*, **13**, 304–326.
- Thompson, R.L., 1998: Eta model storm-relative winds associated with tornadic and nontornadic supercells. *Wea. Forecasting*, **13**, 125–137.
- Thompson, R.L., R. Edwards, J.A. Hart, K.L. Elmore, and P. Markowski, 2003: Close proximity soundings within supercell environments obtained from the rapid update cycle. *Wea. Forecasting*, **18**, 1243–1261.
- Weaver, J. F., 1979: Storm motion as related to boundary-layer convergence. *Mon. Wea. Rev.*, **107**, 612–619.
- Weisman, M.L., and R. Rotunno, 2000: The use of vertical wind shear versus helicity in interpreting supercell dynamics. *J. Atmos. Sci.*, **57**, 1452–1472.
- Weisman, M.L., M.S. Gilmore and L.J. Wicker, 1998: The impact of convective storms on their local environment: what is an appropriate ambient sounding?. Preprints, *19th Conf. on Severe Local Storms*, Minneapolis, MN, Amer. Meteor. Soc., 238–688.
- Wilhelmson, R.B., and J.B. Klemp, 1981: A three-dimensional numerical simulation of splitting severe storms on 3 April 1964. *J. Atmos. Sci.*, **38**, 1581–1600.
- Wilks, D. S., 1995: *Statistical Methods in the Atmospheric Sciences*. Academic Press, 467 pp.
- Zehr, R.M., and J.F.W. Purdom, 1982: Examples of a wide variety of thunderstorm propagation mechanisms. Preprints, *12th Conf. on Severe Local Storms*, San Antonio, TX, Amer. Meteor. Soc., 499–502.